Applied Catalysis B: Environment and Energy 355 (2024) 124146

Contents lists available at ScienceDirect

Applied Catalysis B: Environment and Energy

journal homepage: www.elsevier.com/locate/apcatb

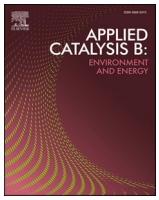

Direct solar-driven electrochemical dissociation of H_2S to H_2 with 12 % solar-to-hydrogen conversion efficiency in diaphragm electrolytic reactor

Chao Duan [a,b,1], Chun Tang [b,c,1], Yonghong Du [b], Shan Yu [b], Heng Guo [b,c], Yu Bai [b], Ying Zhou [a,b,*]

[a] State Key Laboratory of Oil and Gas Reservoir Geology and Exploitation, Southwest Petroleum University, Chengdu 610500, China
[b] School of New Energy and Materials, Southwest Petroleum University, Chengdu 610500, China
[c] Tianfu Yongxing Laboratory, Chengdu 610213, China

ARTICLE INFO

Keywords:
Electrocatalysis
Hydrogen evolution
H_2S splitting
PV-EC system

ABSTRACT

Solar-driven electrochemical dissociation of hydrogen sulfide (H_2S) to hydrogen and sulfur products in photovoltaic-electrochemical (PV-EC) devices becomes an effective strategy for acid gas purification and energy-saving hydrogen production. However, available H_2S splitting electrochemical devices suffer from inferior energy conversion efficiency and fussy multi-step sulfur recovery problems. Herein, we propose an integrated solar-driven PV-EC system with diaphragm electrolytic reactor to solve these challenges. The optimized system integrated commercial silicon solar delivers a high solar-to-hydrogen energy conversion efficiency of up to 12 %, with approximately 99 % H_2 faradaic efficiency and demonstrates at least 50 hours of stability. More importantly, the S^{2-}/HS^- can be transformed into add-valued $Na_2S_2O_3$ by one-step method in Na_2SO_3 media, which avoids complex sulfur recovery. This work presents an alternative method of low-energy consumption for producing H_2 and high-value sulfur-related chemicals by H_2S splitting through a PV-EC system.

1. Introduction

With the development of society, around two-thirds of the global greenhouse gas emissions stem from energy-related sources, emphasizing the imperative to advance renewable energy development [1,2]. In place of dwindling fossil fuels, hydrogen is a carbon-neutral energy transporter, but implementing the hydrogen economy would require effective hydrogen production [3]. Direct solar-driven electrochemical water splitting to produce green hydrogen has been investigated as an attractive technology for low-cost renewable hydrogen [4–10], especially with the rapid growth of photovoltaic power capacity. However, the slow four-electron transfer of the anodic oxygen evolution reaction (OER) is the cause of high overall electricity consumption. Based on this, the hybrid electrochemical water splitting system has received extensive attention, which couples cathodic hydrogen evolution reaction (HER) with a more thermodynamically efficient anodic oxidation, offering a viable strategy for less energy-intensive hydrogen production [11–18].

Hydrogen sulfide (H_2S), as one of the significant industrial exhaust gas, generate about ten million tons per year from natural phenomena and human activities and is expected to increase further in chemical feedstocks such as natural gas, syngas, and refinery gas [19]. At the same time, as an important resource, H_2S is also a promising hydrogen and sulfur source [20]. The thermodynamic potential for H_2S oxidation only needs 0.14 V compared to H_2O splitting (1.23 V in theory), which extremely improves the overall energy efficiency [21–23]. Electrochemical synthesis of green hydrogen and valued sulfur-related products by consuming H_2S, potential resources of hydrogen and sulfur, represents a promising pathway for economic sustainability [24–26]. Especially, direct solar-driven electrochemical dissociation of H_2S to H_2 and valued sulfur-related products. It utilizes solar energy as electricity input with low-energy consumption and is operated under mild reaction conditions, compared to the traditional H_2S energy-intensive purification Claus process, in which elevated high temperatures and not reclaimed H_2.

The novel pathway for acid gas purification driven by solar energy realizes the coupling utilization of new energy and traditional fossil

* Correspondence to: State Key Laboratory of Oil and Gas Reservoir Geology and Exploitation, School of New Energy and Materials, Southwest Petroleum University, Chengdu 610500, China.
E-mail address: yzhou@swpu.edu.cn (Y. Zhou).
[1] The authors contributed equally to this work.

https://doi.org/10.1016/j.apcatb.2024.124146
Received 20 February 2024; Received in revised form 28 March 2024; Accepted 30 April 2024
Available online 3 May 2024

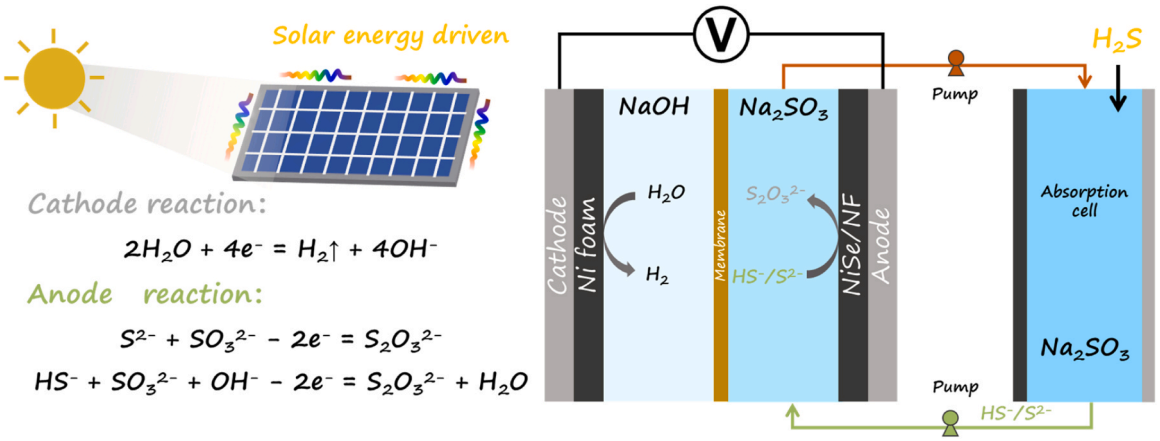

Scheme 1. Direct solar-driven electrochemical dissociation of H_2S to H_2 and high-valued sulfur product.

energy [27–38]. To realize the further application of solar hydrogen, designing a continuous H_2S dissociation device that can contribute to producing green H_2 and simultaneously storing solar energy is crucial. Recently, Li et al [39]. reported an indirect electrochemical-chemical loop strategy for the overall splitting of H_2S to H_2 and elemental sulfur using the intermediate redox media (Fe^{2+}/Fe^{3+}). Despite achieving decomposition of H_2S to produce hydrogen and sulfur, it is limited by needing complex redox reagents and unsatisfactory long-term stability in strong acid environments. Obata et al [40]. studied the same solar-driven indirect H_2S splitting and merely acquired a lower solar-to-hydrogen (STH) conversion efficiency of 1.4 %, far below the STH efficiency of 10 % for commercial applications. The indirect electrochemical-chemical method has not been able to achieve industrial application so far, mainly because of the challenge of anti-corrosion materials in strong acid environments and the system need to introduce additional REDOX reagent [22]. To tackle this dilemma, another promising approach that has attracted increasing attention is the direct electrochemical splitting of H_2S to H_2 and sulfur-based products. With this strategy, the sodium hydroxide (NaOH) solution as an alkali solution to absorb H_2S and then electrocatalytic reaction at the cathode for hydrogen evolution reaction (HER) and anode for sulfide oxidation reaction (SOR). The primary drawback lies in the additional steps required for obtaining sulfur, involving the acidification of the electrolyte, which brings additional cost increases [13]. Moreover, most electrochemical systems of the above studies are still based on traditional H-type cell reactors, thus maintaining a lower mass and energy conversion efficiency. Despite the modest success that has been witnessed in this field, it is still challenging to develop satisfying energy conversion efficiency and low-cost systems by solar-driven energy.

Herein, we propose an innovative approach that continuously splits H_2S for H_2 with a diaphragm electrolytic reactor. In this kind of reactor, the cathode split of water to produce H_2, simultaneously, the anode S^{2-}/HS^- can be one-step transformed into add-valued $Na_2S_2O_3$, avoiding the extra acidification process. In particular, a direct solar-driven PV-EC H_2S splitting system in a diaphragm electrolytic reactor has been designed (schematic diagram and design principle see Scheme 1). The optimized system exhibits approximately 99 % H_2 faradic efficiency and displays at least 50 h stability with a 1.0 V voltage silicon solar cell. Besides, it delivers a solar-to-hydrogen energy conversion efficiency of up to 12 %, outperforming the reported PV-EC H_2S splitting system to the best of our knowledge [32,33]. Besides, compared with water-splitting electricity consumption, the SOR potential of NiSe/NF at 200 mA cm^{-2} is 1.04 V lower than that of OER, indicating lower voltage inputs to driven reaction. Finally, the combination of *in-situ* ATR-FTIR and Raman spectra provide a comprehensive explanation for the reason of the long-term stability without sulfur passivation, because of SOR follows the route of S^{2-}/HS^- to high-valued $Na_2S_2O_3$ product, which act as fixing agent for the photographic industry and detoxification in medicine. This work achieves sustainable production of green H_2 and simultaneous efficient electrocatalysis H_2S splitting solely by solar energy driven.

2. Experiments

2.1. Materials

Sodium sulphite (Na_2SO_3) was purchased from Aladdin Ltd. (Shanghai, China), and other materials details are identical to our previous reports [41].

2.2. Sample preparation

The NiSe/NF catalyst was synthesized by hydrothermal method, and the fabrication process can be found in our published work [41].

2.3. Materials characterization

X-ray diffraction data were collected using Philips X'Pert diffractometer with Cu Kα radiation (λ=1.5418 Å) to analyze the self-supporting NiSe/NF crystal structure. Morphology observation of the NiSe/NF catalyst were conducted by scanning electron microscopy (SEM, ZEISS Sigma 300). Transmission electron microscopy (TEM) characterizations were obtained within FEI TECNAI G20.

2.4. Electrochemical measurement

In a three-electrode system, the electrochemical tests were performed by 50 mL H-cell type cell with graphite rod and Hg/HgO electrode as the counter and reference electrodes severally (CHI 660D electrochemical analyzer). The electrode potential in this paper was represented in reversible hydrogen electrode scale using following equation:

$$E\ (RHE) = E\ (Hg/HgO) + 0.098\ V + 0.0591 * pH \quad (1)$$

1 M Na_2SO_3, Na_2S/NaOH, and Na_2S/Na_2SO_3 solutions were used as electrolyte for LSV tests with a scan rate of 5 mV s^{-1}. The electrochemical measurements in solar-driven H_2S splitting PV-EC reactor were measured in a two-electrode system, and the long-term durability was tested by Keithley 2400 Source Meter.

2.5. In situ attenuated total reflection Fourier transform infrared (ATR-FTIR) and Raman tests

ATR-FTIR was performed (Bruker infrared spectrometer (Tensor II)) to get into the sulfide oxidation reaction mechanism. The Pike VeeMAX

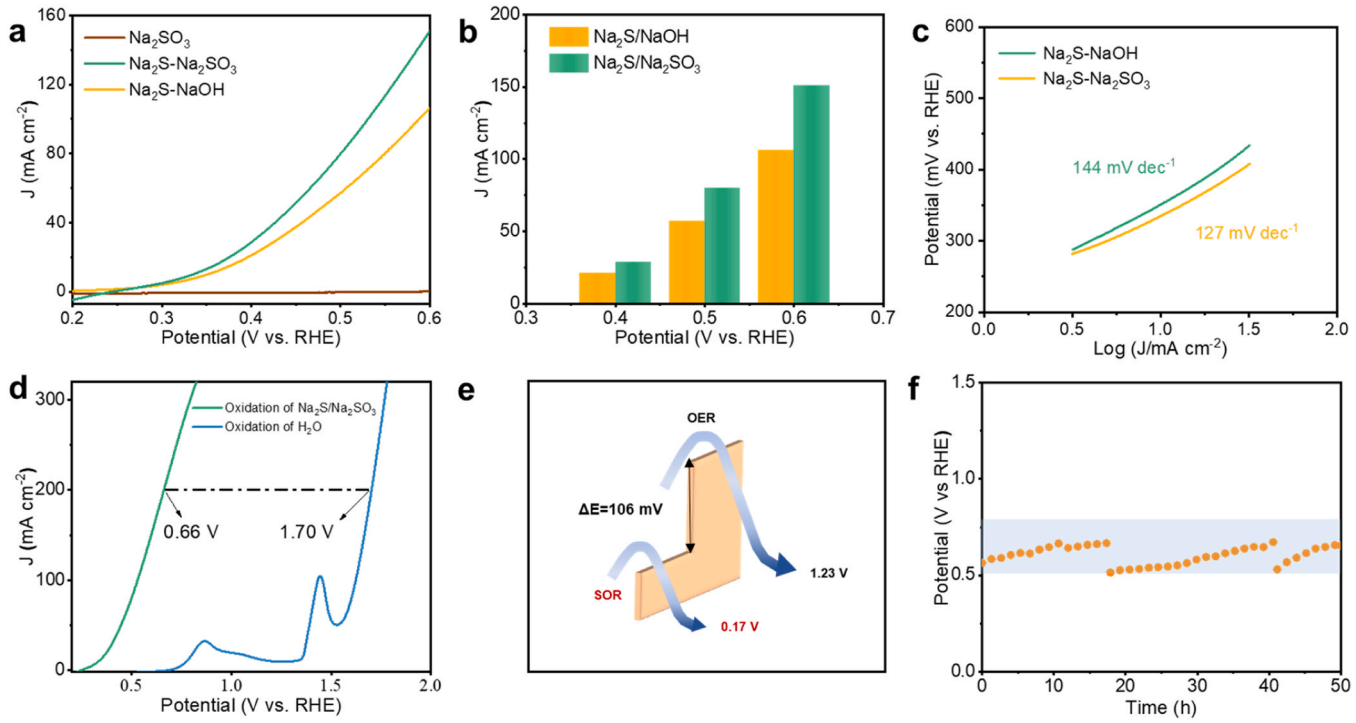

Fig. 1. (a) LSV polarization curves of NiSe/NF in Na_2SO_3, Na_2S/NaOH, and Na_2S/Na_2SO_3 solutions for SOR. (b) Corresponding current densities at different potentials. (c) Tafel plots of NiSe/NF in Na_2S/NaOH and Na_2S/Na_2SO_3. (d) Comparison of the SOR and OER LSV curves of the NiSe/NF electrode. (e) A theoretical voltage of SOR and OER. (f) Potential-time curve of NiSe/NF at 100 mA cm^{-2} for 50 h durability.

III variable angle accessory,in conjunction with a custom-made electrochemical cell setup, was utilized, featuring a Ge crystal. To explore the SOR mechanism deeply, the Raman spectrometer equipped with 473 nm laser excitations (Horiba Lab Ram HR) was carried out to detect sulfur-related species comprehensively.

2.6. Solar-to-hydrogen conversion efficiency calculation

For the direct solar-driven H_2S Splitting PV-EC system, the solar-to-hydrogen conversion efficiency (η_{STH}) was calculated according to the following formula:

$$\eta_{STH} = \frac{Standard\ molar\ enthalpy\ of\ combustion(kJ/mol) \times H_2\ (mol)}{Illumination\ power(W) \times Time(s)} \quad (2)$$

Here, the formula is calculated by the standard molar enthalpy of combustion (237 kJ/mol at 25℃) to measure the energy of H_2. The power of the light source can be measured directly by the optical power meter (PM 100D, Thorlabs, America). The input energy of the system can be obtained by multiplying the optical power by the corresponding irradiation area of the solar cell. The ratio of hydrogen energy to input energy is the STH conversion efficiency.

2.7. H_2 evolution measurement

The rate of H_2 evolution was evaluated in H-type cells using Techcomp Instrument Co., Ltd. GC-7900 gas chromatography with galvanostatic test at 100 mA/cm^2. Prior to the reaction, the electrolyte was bubbled with Ar for 30 min to evacuate O_2 and 1 mL pure CH_4 gas injected into the electrolytic tank as internal standard. Then 0.2 mL of gas is extracted with a syringe from the electrolytic tank and injected into the gas chromatography every 10 min. Quantification of the H_2 was performed using the thermal conductivity detector (TCD). In solar-driven H_2S Splitting PV-EC system, H_2 was collected by drainage method.

Calculation of the H_2 Faradaic efficiency ($\mathbf{FE_{H2}}$): The $\mathbf{FE_{H2}}$ are calculated from gas chromatography chromatogram peak areas at different time in points as follow:

$$FE_{H_2} = \frac{2nF}{It} \times 100\% \quad (3)$$

n: Quantity of H_2, mol;
F: Faradaic constant, 96485 C mol^{-1};
I: Current, A;
t: Time, s

2.8. Direct solar-driven H_2S Splitting PV-EC system measurement

NiSe/NF (2×2 cm^2) as the anode and Ni foam (2×2 cm^2) as the cathode. 1 M NaOH catholyte and 1 M Na_2S/Na_2SO_3 anode electrolyte were pumped into flow cell. All the tests were in a flow cell with 170 mL/min at 25 ℃. STH tests were powered by a commercial solar cell under simulated AM 1.5 G solar irradiation (100 mW cm^{-2}).

3. Results and discussion

3.1. Structural characterization of NiSe/NF

As schematically illustrated in Fig. S1, NiSe/NF was prepared through one-step hydrothermal process. Additionally, images taken using a scanning electron microscope (SEM) and a transmission electron microscope (TEM) reveal the surface nanowire array morphologies of NiSe/NF (Fig. S2b-d). The (300) and (101) planes of NiSe can be matched well with interplanar distances of 2.82 and 3.00 Å respectively (Fig. S2g). By X-ray diffraction (XRD) analysis, the crystal structure of NiSe/NF was discovered. The XRD pattern intuitively displays the peaks corresponding to NiSe (PDF No. 18–0887) [41,42]. In general, the above results prove the successful synthesis of the NiSe/NF catalyst through a hydrothermal process.

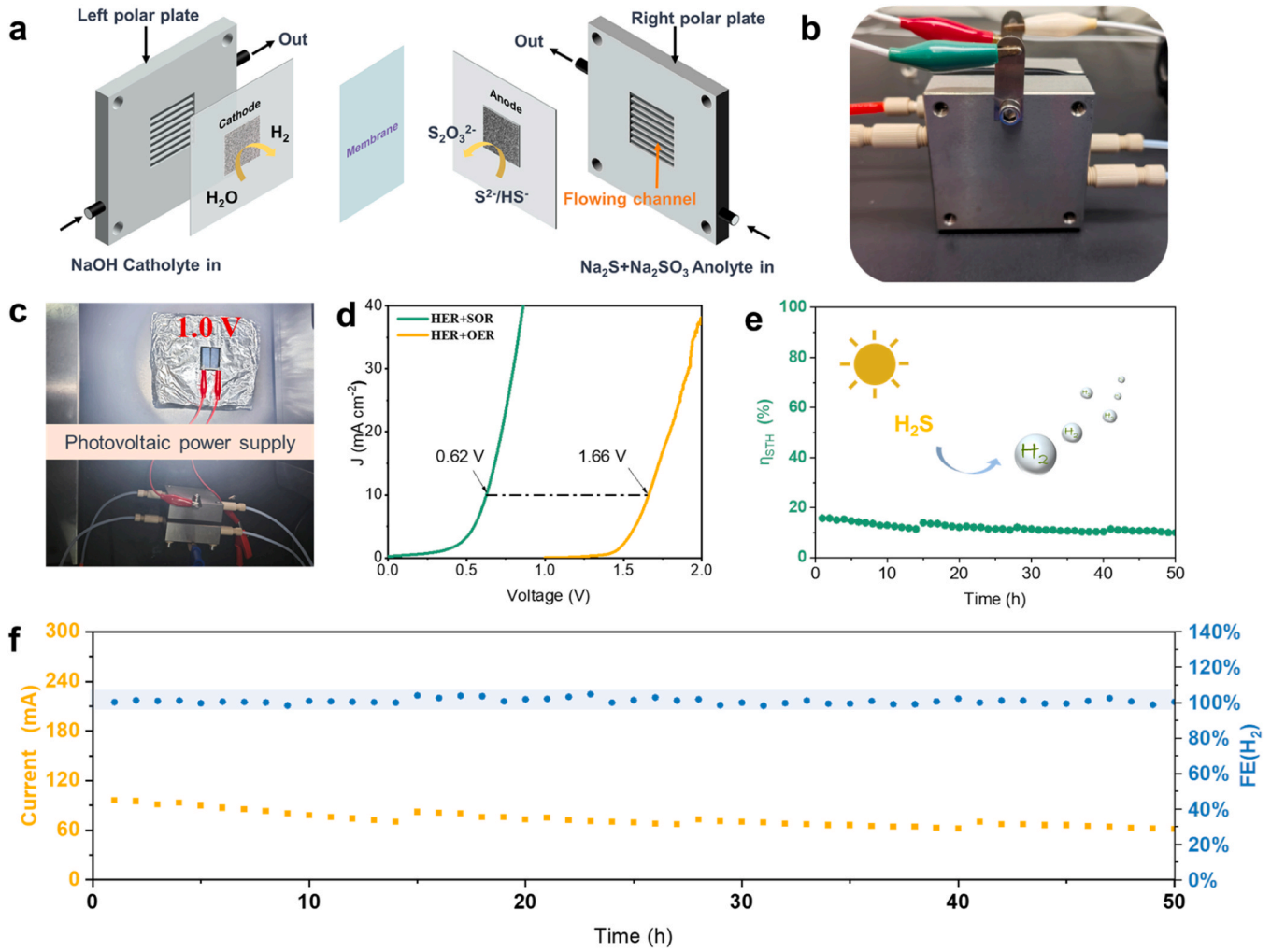

Fig. 2. (a) Schematic diagram of the two-electrode electrolyzer in a flow reactor. (b-c) Photograph of the flow cell integrated with a solar-driven H_2S splitting system. (d) LSV curves of the hybrid HER and SOR of NiSe/NF. (e) Stability curve of solar to hydrogen conversion efficiency. (f) Overall current and H_2 Faraday efficiency in the electrolysis process.

3.2. Electrocatalytic performance

Elctrocatalytic activities of as-prepared NiSe/NF catalyst were studied in 1 M NaOH and 1 M different electrolytes (1.0 M Na_2SO_3, Na_2S/NaOH, and Na_2S/Na_2SO_3) using a standard three-electrode system. First, Linear sweep voltammetry (LSV) at a scan rate of 5 mV/s was used to assess SOR activity. According to Fig. 1a, NiSe/NF electrode exhibits great SOR activity in Na_2S/Na_2SO_3 solution. In stark contrast, at the same potential window, it displays a minimal current density in 1.0 M Na_2SO_3 media, NiSe/NF exhibits the best electrochemical activity in 1.0 M Na_2S/Na_2SO_3 solution. Moreover, the SOR performances were compared quantitatively using the achieved current density at different potentials. Fig. 1b exhibits the current densities of NiSe/NF catalyst at potentials of 0.4 V, 0.5 V, 0.6 V. The current density of NiSe/NF reaches 151.0 mA cm^{-2} at 0.6 V in Na_2S/Na_2SO_3 solution, which is higher than the current density in Na_2S/NaOH solution (106.4 mA cm^{-2}), revealing the superior SOR performance of NiSe/NF in Na_2S/Na_2SO_3 media. Cyclic voltammetry (CV) in 1 M Na_2SO_3 and 1 M Na_2S/Na_2SO_3 electrolyte respectively were conducted to exploration the redox process. As shown in Fig. S3a, there is a redox peak between 0.6 and 1.0 V vs. RHE corresponding to Ni^0/Ni^{2+} for conductive substrate of Ni foam. And there is no redox peak assigned to the oxidized of NiSe, indicating NiSe/NF cannot be oxidized during the potential range of 0–0.6 V vs. RHE. Then, the redox process in the Na_2S/Na_2SO_3 solution was studied using CV in a wide voltage window. Fig. S3b shows oxidation peak between 0 and 1.1 V potential consistent with the SOR reaction. With the potential increases, the current cannot continue to increase due to diffusion limitations. And the oxidation peak between 1.4 and 2.0 V corresponds to the OER reaction with the potential further increases.

Tafel plots were derived from the LSV curves for evaluation of the kinetic mechanism of SOR. The Tafel slope of SOR in Na_2S/Na_2SO_3 (127 mV dec^{-1}) was found to be smaller than that in Na_2S/NaOH media (144 mV dec^{-1}), as shown in Fig. 1c. This indicates that the kinetics more favorable in Na_2S/Na_2SO_3 than in Na_2S/NaOH on NiSe/NF. Fig. 1d suggests that the potential of NiSe/NF for OER is 1.70 V at 200 mA cm^{-2}. Interestingly, the potential sharply decreases to 0.66 V for the SOR reaction. This observation implies that the SOR reaction plays a crucial role in improving the electrocatalytic performance of the NiSe/NF catalyst. The reduction in potential indicates more efficient utilization of energy, which is essential for practical applications (Fig. 1e). Besides, the HER performance of the NiSe/NF cathode catalyst is also explored as shown in Fig. S4. Notably, the catalyst is highly stable at least for 50 h witnessed from its chronoamperometric studies (Fig. 1f). The periodical change of stability are due to replacing the electrolyte (every ca. 20 h). Therefore, the efficient catalytic activity of NiSe/NF in 1.0 M Na_2S/Na_2SO_3 prompts us to further design the PV-EC diaphragm electrolytic reactor and explore its performance in flow cells.

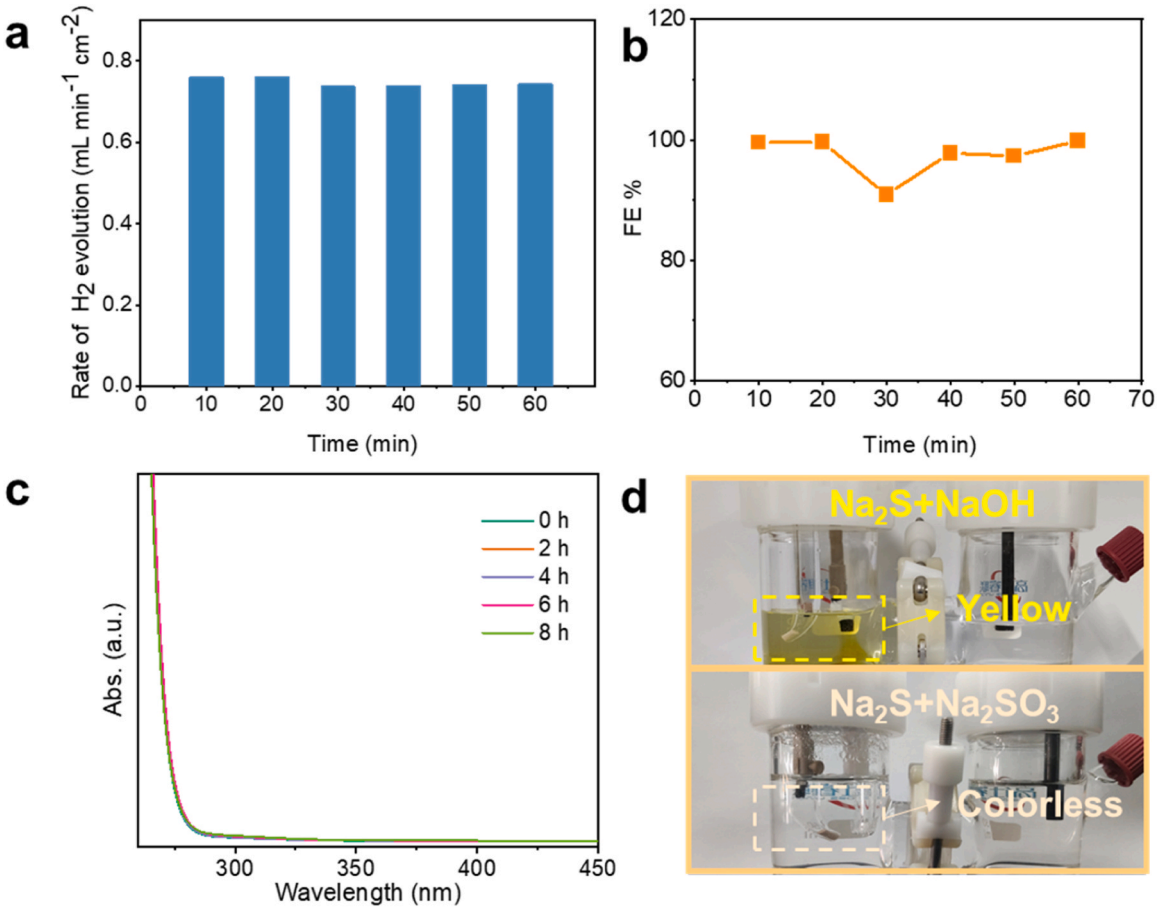

Fig. 3. (a-b) H_2 generation rates and Faradaic efficiencies during a galvanostatic test at a current density of 100 mA cm^{-2}. (c) UV-Vis spectra of electrolytes at various times. (d) Digital photograph of the different electrolyte conditions.

3.3. Direct solar-driven H_2S splitting PV-EC system

Except for exploring the performance and stability of SOR reaction, we further established a flow electrolytic cell for H_2S splitting integrated solar-driven PV-EC system. Figs. 2a and 2b display a diaphragm flow electrolytic reactor, which is assembled by employing the NiSe/NF (2×2 cm^2) as anode and Ni foam (2×2 cm^2) as cathode. 1 M NaOH catholyte and 1 M Na_2S/Na_2SO_3 anolyte were fed into the flow cell by a peristaltic pump, respectively. The polar plate includes flowing channels that the electrolyte is driven by the pump into the flow channels and reacted with the electrode. The proton exchange membrane can separate the reactants, making the products easy to collect. Moreover, the effect of temperature and the flow rate of electrolytes for SOR in the PV-EC system was investigated. Firstly, the relationship between pump revolutions and the flow rates of electrolyte was explored. The revolutions of 100, 200, and 300 per minute respond to flow rates of 54, 114, and 170 mL/min of electrolyte (Fig. S5a). The current gradually increases with the increases of revolutions and temperatures, suggesting the kinetics of SOR was improved, as shown in Fig. S5b-c.

Then, the Na_2S/Na_2SO_3 media is used to simulate the absorbed H_2S solution. Fig. 2c demonstrates the direct solar-driven H_2S splitting system assembled with a commercial Si solar cell with 1.0 V voltage. Notably, the polarization curves show that the splitting H_2S by NiSe/NF only needs ultralow 0.62 V voltage to drive H_2 production, which is 1.04 V lower than that of splitting water to generation H_2 (Fig. 2d). H_2 was collected by drainage method under simulated AM 1.5 G solar irradiation (100 mW cm^{-2}). As shown in Fig. 2e, the $\eta_{STH,}$ is ca. 12.0 %, approaching the highest H_2S splitting performance reported to date [39, 40].

Furthermore, overlaying the J-V curve of commercial Si solar cell tandem with the LSV curve of the two-electrode catalyst system to analyze the performance of the integrated system, which can operate at a current density of around 77 mA and an average photovoltage of 0.71 V (Fig. S6). For comparation, the STH for water splitting in diaphragm reactor was also conducted. The water splitting system cannot driven by a 1.0 V commercial solar cell, which indicates the splitting of H_2S is indeed an energy-saving system. Subsequently, a 2.0 V commercial solar cell was used to test water splitting (Fig. S7), operating at a current density of around 60 mA with STH of ~8 %. The splitting of H_2S system is also relatively stable with a 1.0 V voltage solar cell, the current slightly fluctuates due to the S^{2-}/HS^- ions concentration decrease during the reaction, and the total current is average 72 mA during 50 h test and H_2 faradic efficiency 99 % by calculation (Fig. 2f). Besides, the traditional H-type electrolytic cell was also explored for full H_2S splitting under the same solar irradiation, the total current is average 18 mA and H_2 faradic efficiency 97 %, which exhibits lower η_{STH} efficiency with ca. 3.0 % by calculation (Fig. S8). In comparison to the H-type electrolytic cell, the diaphragm electrolytic reactor has a lower electrolyzer voltage and fast energy/mass transport efficiency, promoting a solar Si cell integrating flow electrolytic reactor of PV-EC H_2S splitting system with highly efficient η_{STH} conversion.

Besides, to explore the impact of photovoltaic volatility on the system, the stability of NiSe/NF was explored by the multi-potential steps method. Fig. S9 shows that NiSe/NF remains excellent stability at different current densities. The difference between real online H_2S absorption and Na_2S solution in the system also studied, Firstly, a homemade device was used to produce H_2S by reaction of 1.0 M Na_2S and 2 M HCl solution, then the H_2S flowed to the Na_2SO_3 solution. As

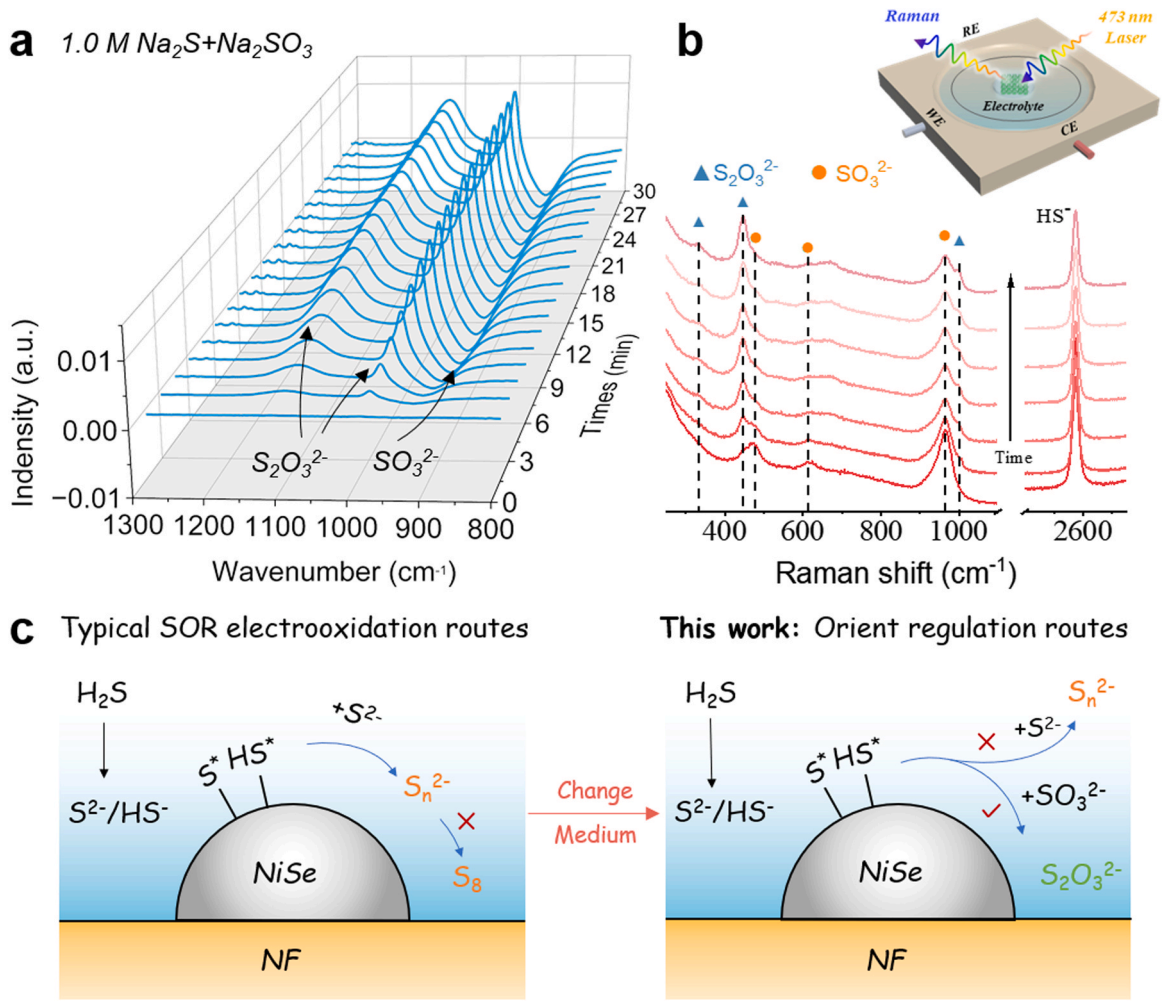

Fig. 4. (a) Schemes of *in situ* ATR-FTIR spectroscopy and (b) *in situ* Raman spectra for NiSe/NF in 1.0 M Na_2S and Na_2SO_3 media during 30 min at 0.627 V. (c) Diagram of sulfide oxidation reaction pathways over NiSe/NF catalyst in various reaction media.

presented in Fig. S10, a comparison of polarization curves between simulated 1 M Na_2S-Na_2SO_3 solution and H_2S saturated Na_2SO_3 solution, the current density at 1.2 V is very close, indicating that the simulated experiment is consistent with the real H_2S in 1 M Na_2SO_3 solution. Thus, the successful demonstration of this solar-driven H_2S splitting system is expected to promote green H_2 production and energy storage.

3.4. Products investigation

Following the discovery of a workable method for converting solar energy into hydrogen using a PV-EC system in a diaphragm reactor, the reason for long-term stability was further explored. Firstly, the product in both anode and cathodic were detected respectively. In Fig. 3a-b,.we performed a galvanostatic test on the cathode at a current density of 100 mA cm^{-2}; the H_2 generation rate stayed at roughly 0.77 mL min^{-1} cm^{-2}, extrapolating an average H_2 faradaic efficiency of 98.8 %. For the anode, the products were studied in the electrolyte by UV–vis. Fig. 3c reveals that no the chain polysulfides (S_2^{2-}-S_n^{2-}) peaks are shown at ~300 nm and ~370 nm [27,34,41]. In addition, the anodic electrolyte is still colorless as the reaction proceeds as shown in Fig. S11. Otherwise, Fig. 3d shows Na_2S/NaOH and Na_2S/Na_2SO_3 electrolyte color comparison images during the reaction process.

3.5. Mechanism of electrocatalytic SOR reaction

The SOR reaction pathways in the Na_2SO_3 electrolyte are revealed using *in situ* electrochemical ATR-FTIR and Raman spectroscopy techniques. At present, SOR chain-growing (S^{2-}/HS^- →S_2^{2-} → S_n^{2-}→ S_8*→ S_8) is the main reaction mechanism at NaOH electrolytes, it is worth noting that these polysulfide intermediates can be detected by UVs and Raman. Interestingly, there is no peak of polysulfide detected by UVs which demonstrates a new SOR reaction pathway in Na_2SO_3 electrolyte. Before the *in situ* test, both FTIR and Raman are used to analyze several sulfur-related species (Table S1). As shown in Fig. 4a, the peak at 1117 cm^{-1} and 997 cm^{-1} matching with the S-O stretching vibration of $S_2O_3^{2-}$ increases as sulfide oxidation progresses at 0.627 V, while the S═O vibration of SO_3^{2-} rapidly declines over time, indicating that $S_2O_3^{2-}$ is final species in the Na_2SO_3 media after electro-oxidation. Similar evident peaks with amplification may be seen in Fig. 4b Raman spectra. Among these, the $S_2O_3^{2-}$ species are identified by the signals at 443 cm^{-1}, 663 cm^{-1}, and 993 cm^{-1} [41,43]. The peak strength of $S_2O_3^{2-}$ similarly rises with the potential increase, which is the same as the results of ATR-FTIR spectroscopy. Furthermore, the signal at 2571 cm^{-1} is assigned to the H-S vibration of HS^-, and the peak intensity of HS^- decreases as the reaction progresses, which indicates HS^- is involved in the SOR reaction [41]. As a result, the pathway of SOR can be obtained from Eqs. (4) to (5) as follows:

$$S^{2-} + SO_3^{2-} \rightarrow S_2O_3^{2-} + 2e^- \quad (4)$$

$$2HS^- + SO_3^{2-} + OH^- \rightarrow S_2O_3^{2-} + H_2O + 2e^- \quad (5)$$

All of these findings indicate that most of the S^{2-}/HS^- in the Na_2SO_3 solution has been converted to $S_2O_3^{2-}$, as shown in Fig. 4c. This oxidation method shows that S^{2-}/HS^- is directly converted to $S_2O_3^{2-}$ rather than forming chains in solution via a short to long chain pathway, which inhibits the possibility of NiSe/NF undergoing sulfur passivation, thereby enabling hydrogen evolution coupled with concurrent SOR reaction using solar energy. Therefore, it is crucial to harvest, store, and convert solar energy to create a suitable H_2S splitting system. In order to reduce energy consumption, eliminate power supply constraints, and achieve low-cost, pollution-free, and sustainable green hydrogen production.

4. Conclusion

In summary, we propose a continuous direct solar-driven PV-EC H_2S splitting system in a diaphragm electrolytic reactor for green H_2 production and energy storage. In this system, the S^{2-}/HS^- can be transformed into add-valued $Na_2S_2O_3$ by one-step method. Besides, the optimized system exhibits approximately 99 % H_2 faradic efficiency and displays at least 50 h stability with a 1.0 V voltage silicon solar cell. More importantly, the system delivered a solar-to-hydrogen energy conversion efficiency of up to 12 %. Compared with water splitting electricity consumption, the SOR potential of NiSe/NF achieved current density of 200 mA cm^{-2} is 1.04 V lower than that of OER, indicating lower voltage inputs to driven reaction. The combination of *in situ* ATR-FTIR and Raman spectra comprehensively explains the reason for the long-term stability without sulfur passivation, which follows the route of S^{2-}/HS^- to high-valued $Na_2S_2O_3$ product in Na_2SO_3 electrolytes. This work provides an alternative avenue for green H_2 and high-valued sulfur-related chemical production from hazardous H_2S splitting, significantly improving the economic sustainability of the H_2S degradation process.

CRediT authorship contribution statement

Chao Duan: Writing – original draft, Investigation, Conceptualization. **Chun Tang:** Conceptualization, Investigation, Methodology, Project administration, Writing – review & editing. **Shan Yu:** Data curation, Resources, Software. **Yonghong Du:** Investigation, Methodology. **Ying Zhou:** Conceptualization, Funding acquisition, Supervision, Writing – review & editing. **Heng Guo:** Methodology, Resources, Validation. **Yu Bai:** Investigation.

Declaration of Competing Interest

The authors declare that they have no known competing financial interests or personal relationships that could have appeared to influence the work reported in this paper.

Data availability

Data will be made available on request.

Acknowledgement

We gratefully acknowledge financial support from the National Natural Science Foundation of China (No 52325401), Natural Science Foundation of Sichuan (2022NSFSC0023, 23NSFSC0112). Tianfu Yongxing Laboratory Science and Technology Key Project (2023KJGG15).

Appendix A. Supporting information

Supplementary data associated with this article can be found in the online version at doi:10.1016/j.apcatb.2024.124146.

References

[1] Z. Li, S. Fang, H. Sun, R. Chung, X. Fang, J. He, Solar hydrogen, Adv. Energy Mater. 13 (2023) 2203019.
[2] J. Li, C. Tang, H. Zhang, Z. Zou, C.M. Li, Mesoporous molybdenum carbide for greatly enhanced hydrogen evolution at high current density and its mechanism studies, Mater. Rep. Energy 3 (2023) 100215.
[3] J.C. Ehlers, A.A. Feidenhans'l, K.T. Therkildsen, G.O. Larrazábal, Affordable green hydrogen from alkaline water electrolysis: key research needs from an industrial perspective, ACS Energy Lett. 8 (2023) 1502–1509.
[4] I. Holmes-Gentle, S. Tembhurne, C. Suter, S. Haussener, Kilowatt-scale solar hydrogen production system using a concentrated integrated photoelectrochemical device, Nat. Energy 8 (2023) 586–596.
[5] A.M.K. Fehr, A. Agrawal, F. Mandani, C.L. Conrad, Q. Jiang, S.Y. Park, O. Alley, B. Li, S. Sidhik, I. Metcalf, C. Botello, J.L. Young, J. Even, J.C. Blancon, T. G. Deutsch, K. Zhu, S. Albrecht, F.M. Toma, M. Wong, A.D. Mohite, Integrated halide perovskite photoelectrochemical cells with solar-driven water-splitting efficiency of 20.8 %, Nat. Commun. 14 (2023) 3797.
[6] K. Chang, D.T. Tran, J. Wang, K. Dong, S. Prabhakaran, D.H. Kim, N.H. Kim, J. H. Lee, Triphasic Ni_2P-Fe_2P-CoP heterostructure interfaces for efficient overall water splitting powered by solar energy, Appl. Catal. B Environ. 338 (2023) 123016.
[7] M.M. Meshesha, D. Chanda, R. Balu, S.G. Jang, S. Ahmed, B.L. Yang, Efficient green hydrogen production through metal–organic framework-derived Ni and Co mediated iron selenide hexagonal nanorods and wireless coupled with photovoltaics for urea and alkaline water electrolysis, Appl. Catal. B Environ. 344 (2024) 123635.
[8] X. Li, X. Wu, B. Li, S. Zhang, Y. Liu, Z. Li, D. Zhang, X. Wang, Q. Sun, D. Gao, C. Zhang, W.-H. Huang, C.-C. Chueh, C.-L. Chen, S. Yang, S. Xiao, Z. Wang, Z. Zhu, Efficient Solar-Driven Water Splitting Enabled by Perovskite Photovoltaics and a Halogen-Modulated Metal–Organic Framework Electrocatalyst, ACS Nano 17 (2023) 23478–23487.
[9] R. Fan, C. Liu, Z. Li, H. Huang, J. Feng, Z. Li, Z. Zou, Ultrastable electrocatalytic seawater splitting at ampere-level current density, Nat. Sustain. 7 (2024) 148–157.
[10] H. Song, S. Luo, H. Huang, B. Deng, J. Ye, Solar-driven hydrogen production: recent advances, challenges, and future perspectives, ACS Energy Lett. 7 (2022) 1043–1065.
[11] T. Wang, X. Cao, L. Jiao, Progress in hydrogen production coupled with electrochemical oxidation of small molecules, Angew. Chem. Int. Ed. 61 (2022) e202213328.
[12] J. Du, D. Xiang, K. Zhou, L. Wang, J. Yu, H. Xia, L. Zhao, H. Liu, W. Zhou, Electrochemical hydrogen production coupled with oxygen evolution, organic synthesis, and waste reforming, Nano Energy 104 (2022) 107875.
[13] X. Liu, Y. Han, Y. Guo, X. Zhao, D. Pan, K. Li, Z. Wen, Electrochemical hydrogen generation by oxygen evolution reaction-alternative anodic oxidation reactions, Adv. Energ. Sust. Res. 2200005 (2022) 1–27.
[14] R. Li, K. Xiang, Z. Peng, Y. Zou, S. Wang, Recent advances on electrolysis for simultaneous generation of valuable chemicals at both anode and cathode, Adv. Energy Mater. 11 (2021) 2102292.
[15] D. Yan, C. Mebrahtu, S. Wang, R. Palkovits, Innovative electrochemical strategies for hydrogen production: from electricity input to electricity output, Angew. Chem. Int. Ed. 62 (2022) e202214333.
[16] Y. Xu, B. Zhang, Recent advances in electrochemical hydrogen production from water assisted by alternative oxidation reactions, ChemElectroChem 6 (2019) 3214–3226.
[17] X. Liu, K. Deng, P. Liu, X. Lv, W. Tian, K. Ma, H. Li, J. Ji, Mutual promotion by structural design and intrinsic activity coupling of CNTs/MoC/CoNiMo for water splitting and urea electrolysis, Appl. Catal. B Environ. 343 (2024) 123470.
[18] X. Xu, H. Liao, L. Huang, S. Chen, R. Wang, S. Wu, Y. Wu, Z. Sun, H. Huang, Surface reconstruction and directed electron transport in $NiSe_2/MoSe_2$ Mott-Schottky heterojunction catalysts promote urea-assisted water splitting, Appl. Catal. B Environ. 341 (2024) 123312.
[19] H. Yang, J. Bai, T. Zhou, C. Zhou, C. Xie, Y. Zhang, J. Li, A. Simchi, B. Zhou, Electrochemical coupling conversion of sulfur-containing gaseous waste to treasure: a key review, Appl. Catal. A-Gen. 654 (2023) 119085.
[20] K. Kim, C. Lee, Recent progress in electrochemical hydrogen sulfide splitting: strategies for enabling Sulfur-tolerant anodic reactions, Chem. Eng. J. 469 (2023) 143861.
[21] Z. Zhang, Y. Lei, W. Huang, Recent progress in carbon-based materials boosting electrochemical water splitting, Chin. Chem. Lett. 33 (2022) 3623–3631.
[22] X. Ren, J. Shi, R. Duan, J. Di, C. Xue, X. Luo, Q. Liu, M. Xia, B. Lin, W. Tang, Construction of high-efficiency $CoS@Nb_2O_5$ heterojunctions accelerating charge transfer for boosting photocatalytic hydrogen evolution, Chin. Chem. Lett. 33 (2022) 4700–4704.
[23] K. Sun, Y. Zhao, J. Yin, J. Jin, H. Liu, P. Xi, Surface modification of $nico_2o_4$ nanowires using organic ligands for overall water splitting, Acta Phys. -Chim. Sin. 38 (2022) 136–143.
[24] M. Ferree, J. Kosco, F. Laquai, A. Cavazos Sepulveda, D.P. San Roman Alerigi, Solar fuel production from hydrogen sulfide: an upstream energy perspective, Adv. Energ. Sust. Res. 4 (2023) 2200201.
[25] Y.H. Chan, A.C.M. Loy, K.W. Cheah, S.Y.W. Chai, L.H. Ngu, B.S. How, C. Li, S.S. M. Lock, M.K. Wong, C.L. Yiin, B.L.F. Chin, Z.P. Chan, S.S. Lam, Hydrogen sulfide

(H_2S) conversion to hydrogen (H_2) and value-added chemicals: progress, challenges and outlook, Chem. Eng. J. 458 (2023) 141398.
[26] A.G. De Crisci, A. Moniri, Y. Xu, Hydrogen from hydrogen sulfide: towards a more sustainable hydrogen economy, Int. J. Hydrog. Energy 44 (2019) 1299–1327.
[27] M. Zhang, J. Guan, Y. Tu, S. Chen, Y. Wang, S. Wang, L. Yu, C. Ma, D. Deng, X. Bao, Highly efficient H_2 production from H_2S *via* a robust graphene-encapsulated metal catalyst, Energy Environ. Sci. 13 (2020) 119–126.
[28] Y. Pei, J. Cheng, H. Zhong, Z. Pi, Y. Zhao, F. Jin, Sulfide-oxidation-assisted electrochemical water splitting for H_2 production on a bifunctional Cu_2S/nickel foam catalyst, Green. Chem. 23 (2021) 6975–6983.
[29] S. Zhang, Q. Zhou, Z. Shen, X. Jin, Y. Zhang, M. Shi, J. Zhou, J. Liu, Z. Lu, Y. Zhou, H. Zhang, Sulfophobic and Vacancy Design Enables Self-Cleaning Electrodes for Efficient Desulfurization and Concurrent Hydrogen Evolution with Low Energy Consumption, Adv. Funct. Mater. 31 (2021) 2101922.
[30] M. Kumar, T.C. Nagaiah, Efficient production of hydrogen from H_2S *via* electrolysis using a $CoFeS_2$ catalyst, J. Mater. Chem. A 10 (2022) 7048–7057.
[31] M. Kumar, T.C. Nagaiah, Pure hydrogen and sulfur production from H_2S by an electrochemical approach using a NiCu-MoS_2 catalyst, J. Mater. Chem. A 10 (2022) 13031–13041.
[32] Y. Li, Y. Duan, K. Zhang, W. Yu, Efficient anodic chemical conversion to boost hydrogen evolution with low energy consumption over cobalt-doped nickel sulfide electrocatalyst, Chem. Eng. J. 433 (2022) 134472.
[33] L. Zhang, Z. Wang, J. Qiu, Energy-saving hydrogen production by seawater electrolysis coupling sulfion degradation, Adv. Mater. 34 (2022) 2109321.
[34] Z. Xiao, C. Lu, J. Wang, Y. Qian, B. Wang, Q. Zhang, A. Tang, H. Yang, Bifunctional Co_3S_4 nanowires for robust sulfion oxidation and hydrogen generation with low power consumption, Adv. Funct. Mater. 33 (2022) 2212183.
[35] A. Jiang, H. Guo, S. Yu, F. Zhang, T. Shuai, Y. Ke, P. Yang, Y. Zhou, Dual charge-accepting engineering modified $AgIn_5S_8$/CdS quantum dots for efficient photocatalytic hydrogen evolution overall H_2S splitting, Appl. Catal. B Environ. 332 (2023) 122747.
[36] M. Dan, J. Xiang, J. Yang, F. Wu, C. Han, Y. Zhong, K. Zheng, S. Yu, Y. Zhou, Beyond hydrogen production: solar-driven H_2S-donating value-added chemical production over $Mn_xCd_{1-x}S$/$CdyMn_{1-y}S$ catalyst, Appl. Catal. B Environ. 284 (2021) 119706.
[37] Z. Xie, S. Yu, X.-B. Fan, S. Wei, L. Yu, Y. Zhong, X.-W. Gao, F. Wu, Y. Zhou, Wavelength-sensitive photocatalytic H_2 evolution from H_2S splitting over g-C_3N_4 with S,N-codoped carbon dots as the photosensitizer, J. Energy Chem. 52 (2021) 234–242.
[38] M. Dan, S. Yu, Y. Li, S. Wei, J. Xiang, Y. Zhou, Hydrogen sulfide conversion: how to capture hydrogen and sulfur by photocatalysis, J. Photochem. Photobiol. C 42 (2020) 100339.
[39] W. Ma, J. Han, W. Yu, D. Yang, H. Wang, X. Zong, C. Li, Integrating perovskite photovoltaics and noble-metal-free catalysts toward efficient solar energy conversion and H_2S splitting, ACS Catal. 6 (2016) 6198–6206.
[40] K. Obata, Y. Shinohara, S. Tanabe, I. Waki, K. Kotsovos, K. Ohkawa, K. Takanabe, A stand-alone module for solar-driven H_2 production coupled with redox-mediated sulfide remediation, Energy Technol. 7 (2019) 1900575.
[41] C. Duan, C. Tang, S. Yu, L. Li, J. Li, Y. Zhou, Efficient electrocatalytic desulfuration and synchronous hydrogen evolution from H_2S via anti-sulfuretted NiSe nanowire array catalyst, Appl. Catal. B Environ. 324 (2023) 122255.
[42] C. Tang, N. Cheng, Z. Pu, W. Xing, X. Sun, NiSe nanowire film supported on nickel foam: an efficient and stable 3d bifunctional electrode for full water splitting, Angew. Chem. Int. Ed. 54 (2015) 9351–9355.
[43] S. Yu, F. Wu, P. Zou, X.-B. Fan, C. Duan, M. Dan, Z. Xie, Q. Zhang, F. Zhang, H. Zheng, Y. Zhou, Highly value-added utilization of H_2S in Na_2SO_3 solution over Ca-CdS nanocrystal photocatalysts, Chem. Commun. 56 (2020) 14227–14230.